Structural investigation of Ge-As-Se glasses

M. V. POPOVYCH[1,*], A. V. STRONSKI[1], L. O. REVUTSKA[2], K. V. SHPORTKO[1], Y. POLISHCHUK[1], O. P. PAIUK[1], V. YU. GORONESKUL[1]
[1]*V. Lashkaryov Institute of Semiconductor Physics NAS Ukraine, 41 Nauki Ave., 03028 Kyiv, Ukraine*
[2]*National Technical University of Ukraine,"Igor Sikorsky Kyiv Polytechnic Institute", 37 Peremohy Ave., 03056 Kyiv, Ukraine*

In the present paper the amorphous Ge-As-Se alloys have been studied by X-ray diffraction and Raman spectroscopy. The experimental X-ray diffraction pattern confirmed an amorphous nature of studied samples. The obtained radial distribution functions have manifested the evolution of the short range in Ge-As-Se system. The positions of the nearest-neighbour bond length r_1 changed from 2.32 to 2.45 Å with the increase of Ge content. Raman spectra of Ge-As-Se samples revealed that the backbones of the studied samples consist of $AsSe_{3/2}$ pyramidal units, edge- and corner-shared $GeSe_4$ tetrahedral units and structural units containing homopolar bonds. For Se-rich samples Se chains are present. Compositional dependencies of characteristic constituent Raman bands intensities showed that Ge-As-Se samples contain different nanophases whose concentration is changing with the composition.

(Received May 9, 2022; accepted February 14, 2023)

Keywords: Chalcogenide glasses, X-ray diffraction, Radial distribution function, Raman spectroscopy, Nanophases

1. Introduction

Chalcogenide glasses (CG) are non-oxide glasses with unique properties: transparency in IR spectral range, high values of linear and non-linear refractive index, numerous photo-induced effects, etc. These materials have versatile area of practical applications in photonics, optoelectronics, integrated optics [1-2].

Important information concerning the understanding of the structure of covalent glasses could be received when diffraction data, obtained by X-ray diffraction (XRD) and/or neutron diffraction (ND) and extended X-ray absorption fine structure (EXAFS) spectroscopy techniques allowing to find partial pair distribution functions and contribution of atomic pairs in the construction of glass backbone [3-8]. Useful additional information to the XRD data can be extracted from Raman spectroscopy studies [9-13].

Chalcogenide glassy alloys are attractive for both fundamental studies and practical applications. Being essentially covalent materials they are close to the model objects. The variety of structure models [14-17] were proposed for amorphous chalcogenides. Information on the short-range order structure of chalcogenide glasses is particularly valuable in order to establish useful correlations between their structural and macroscopic properties [17]. For example, the theoretical approach based on valence-force field approximation [16] was enough fruitful in the description of the elastic properties of amorphous chalcogenides. Recently, significant efforts in the studies of chalcogenide glasses were applied for nanocomposites materials based on them. As it is known, the photoinduced processes are influenced by the structural properties of CG and films. For that reason, the information about structural peculiarities, in particular the features of the short-range order, can help to improve the composite nanostructures sensitivity and relief formation processes, in particular, for the composites based on the Ge-As-S and Ge-As-Se glasses, which are perspective for photonics applications (direct optical elements fabrication, all-optical signal processing, holography, including digital one, etc.) [9, 13, 18-24].

The aim of this paper therefore is to carry out the study of structural order in the chalcogenide glasses of the Ge-As-Se system ($Ge_{13.5}As_{23.5}Se_{64}$, $Ge_{18}As_{28}Se_{54}$,$Ge_{4.5}As_{14.5}Se_{81}$, $Ge_{27}As_{37}Se_{36}$ chalcogenide glasses, where we have glasses with high and low Se content and close to the stoichiometric (pseudo-binary) compositions), examining the parameters of the local atomic structure as a function of composition *using* XRD and Raman data for calculating and analysis of evolution of structure with composition. The Ge-As-Se system exhibits stronger covalent bond nature due to the similarity of the atomic mass, the atomic radius and the electronegativity of the constituent elements. A deep understanding of composition-structure-property relationship in Ge-As-Se ternary system is thus becoming increasingly important, which can serve as a guideline for materials selection in practical applications. Among those, the Ge-As-Se system is of particular interest because it has an extremely large glass forming region [25, 26], and this is ideal for clarifying the fundamental composition-structure-property relationship in ternary chalcogenide glasses and important for practical applications.

2. Experimental

Studied $Ge_{4.5}As_{14.5}Se_{81}$, $Ge_{13.5}As_{23.5}Se_{64}$, $Ge_{18}As_{28}Se_{54}$,$Ge_{27}As_{37}Se_{36}$ chalcogenide glasses were prepared by standard melt quenching technique.

X-ray diffraction patterns of the powder samples (particle size less than 5 μm) were recorded with use of the X-ray diffractometer with Bragg–Brentano geometry, using CuK_a radiation 1.54178 Å and mounted graphite monochromator for a diffracted beam. The diffraction data were collected in the range of scattering vector magnitudes Q between 0.4 Å and 8 Å ($Q=4\pi \sin\theta/\lambda$). All samples were examined in transmission geometry. All the X-ray experiments were performed at ambient temperature. The diffraction intensities were corrected for the background, incoherent (polarization and absorption) and multiple scattering in the usual ways in order to eliminate the part of radiation which does not carry structural information. The spectra were measured at a constant rate. The Compton scattering was corrected using the values given by Balyuzi [3]. Faber-Ziman [4], total structure factor $S(Q)$ was calculated from the scattering intensity. After Fourier transformation the reduced radial distribution functions G(r) (RDF) were determined, the measured S(Q) using the fast Fourier transform technique [27-30] as follows:

$$G(r) = \frac{2}{\pi}\int_0^{\infty}(S(Q)-1))Q\sin(Qr)dQ \qquad (1)$$

In reality, the data should be multiplied by a modification factor in order to reduce the ripples inevitably introduced due to the finite accessible upper Q value (Q_{max}) in the measurements.Eq.(1) therefore becomes:

$$G(r) = \frac{2}{\pi}\int_0^{Q_{max}}(S(Q)-1))QM(Q)\sin(Qr)dQ \qquad (2)$$

where $M(Q)$ is called the damping factor [29-30].

$G(r)$ may also be expressed directly in real space coordinates to emphasize its relationship with the local atomic density, $\rho(r)$ at a distance r and the bulk atomic density, ρ_0; as follows

$$G(r) = 4\pi r(\rho(r)-\rho_0) \qquad (3)$$

where $\rho(r)$ is the density function, which represents an atomic pair correlation function, and is equal to zero at values of r less than the average nearest neighbor interatomic separation and equal to the average value of density r_0 at very large value of r, where the material becomes homogenous. In between these two limits, ρ_0 for an amorphous solid will exhibit an oscillatory behavior, with peaks in the probability function representing the average interatomic separations. At short distances ($r \leq$ 2Å), see Eq.(3), $G(r)$ should follow the density line ($4\pi r\rho_0$) which is used as a quality check of the data. [29-30]

The radial distribution function (RDF), $RDF(r)$, is defined as the number of atoms lying at distances between r, $r+dr$ from center of an arbitrary origin atom and written as

$$RDF(r) = rG(r) + 4\pi r^2\rho_0 = 4\pi r^2\rho(r) \qquad (4)$$

The function that is used in the determination of atomic distances and co-ordination numbers is the total distribution function:

$$T(r) = \frac{RDF(r)}{r} = 4\pi r\rho(r) \qquad (5)$$

The average coordination number, N, in a spherical shell between radius r_1 and r_2 around any given atom, can be calculated as the number of atoms in the area between r_0 and r', where r_0 is a lower limit of r, below which $\rho(r)$ is zero, and r_0 is the first minimum of $4\pi r^2(r)$. The position of the first peak gives a value for the nearest-neighbour bond length, r_1, and similarly, the position of the second peak gives the next neighbour distance, r_2. The RDF yields only a limited amount of information, restricted essentially to the local structure around a given atom, i.e. bond lengths and bond angles. [29]

In the present work, we were interested in a quantitative description of the chemical short-range order in the $Ge_{4.5}As_{14.5}Se_{81}$, $Ge_{13.5}As_{23.5}Se_{64}$, $Ge_{18}As_{28}Se_{54}$,$Ge_{27}As_{37}Se_{36}$ ternary glasses over a composition range covering Se-rich and Se-deficient compositions. Assuming that pure Ge, As and Se follow the 8 – Z rule, their coordination numbers Ni equal respectively 4, 3 and 2 (Z is the number of outer shell electrons = the number of the group to which the element belongs). Then the compositions cover the range of the theoretical mean coordination number between 2.24 and 3.

$$MCN = \sum_i c_i(8-Z_i) \qquad (6)$$

where c_i is the concentration of the i-th component).

Radial distribution functions, most probable interatomic distances and coordination numbers can be extracted from a model atomic configuration [31].

Raman spectra of Ge-As-S glasses were measured in the spectral range from 50 to 600 cm^{-1} at room temperature using a FRA-106 Raman attachment to Bruker IFS 88 applying the diode pump Nd:YAG laser of ca. 100 mW power and using the liquid nitrogen -cooled Ge detector with the resolution set to 1 cm^{-1} with 256 scans collected in each experiment. The tentative Gaussian decomposition of obtained Raman spectra was prformed using a series of Gaussians peaks with width appropriate for glasses. The frequency assignments of known structural units in As-Se and Ge-Se glasses were used to perform the peak-fitting analyses and to compare the relative contribution of each structural unit in the spectrum of amorphous Ge-As-Se alloys. It is necessary to note that a larger number of vibrational modes contribute to the overall spectrum. We allowed upon fitting the Raman spectra a maximum 2-3cm^{-1} displacement of the peak from the position of the peaks known from the reference literature.

3. Results and discussion

3.1. X-ray diffraction data

The X-ray diffractograms show that the as-prepared samples of the studied $Ge_{13.5}As_{23.5}Se_{64}$, $Ge_{18}As_{28}Se_{54}$, $Ge_{4.5}As_{14.5}Se_{81}$, $Ge_{27}As_{37}Se_{36}$ chalcogenide glasses are amorphous (Fig.1). They contain several broad bands typical for the amorphous state. The position of the first scattering peak denoting the medium range order is prominent at any composition in all the investigated glasses. Radial distribution functions for studied glasses obtained using program the RAD GTK+ [32] are presented in Fig.2. The mean nearest neighbour distances r_{ij} and coordination numbers N_{ij} extracted from the model g_{ij} functions for all compositions studied are presented in Table 1.

Table 1 shows that the positions of the nearest-neighbour bond length r_1 changed from 2.32 to 2.45 Å. For all the investigated glasses the values of the r_2/r_1 ratio are close to 1.6 which is a typical value for a regular tetrahedron structure. Similar r_1 values were observed for Ge-As-Se glasses of other compositions [31,33-35]. Ge–As–Se glasses are characterized by the lack of preferential bonding and behave as random covalent networks: Ge–Ge, Ge–As or As–As bonds can be found in Se-rich compositions while Se–Se bonding remains in strongly Se-deficient glasses as well.

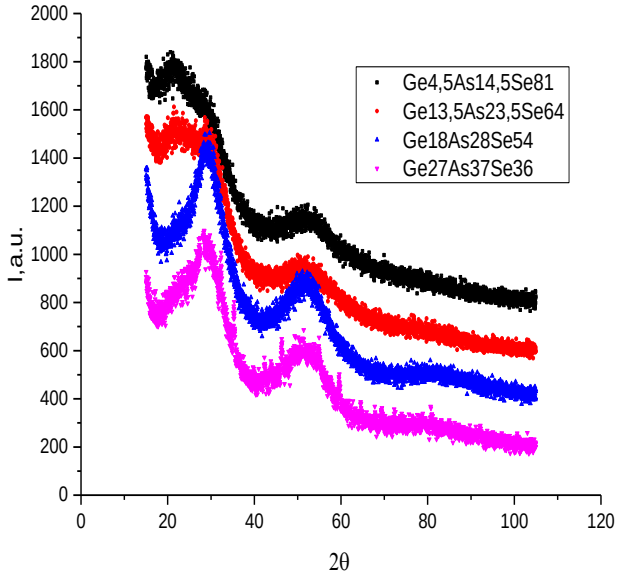

Fig. 1. X-ray diffraction patterns for Ge-As-Se glasses (color online)

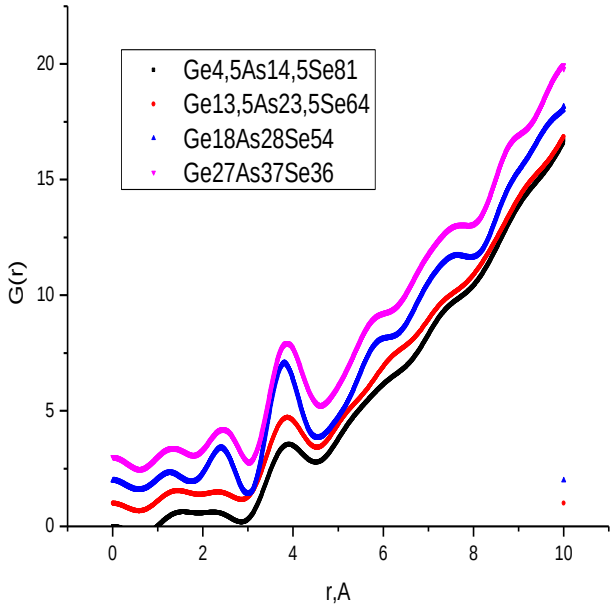

Fig. 2. Radial distribution functions of 4 samples (color online)

The radial distribution functions family of studied Ge−As−Se glasses (see Fig.2 and Table 1 for compositions) show disordered structure.There are Ge−Ge, Ge−As, and As−As bonds in highly selenium-rich compositions and Se−Se bonds in selenium-poor samples, that is both homonuclear and heteronuclear bonds are allowed.

Table 1. Structural parameters of glasses obtained by x-ray diffraction measurements

Composition	r_1 (Å)	r_2 (Å)	*MCN(N)*
$Ge_{4.5}As_{14.5}Se_{81}$	2.32	3.90	2.24
$Ge_{13.5}As_{23.5}Se_{64}$	2.37	3.88	2.525
$Ge_{18}As_{28}Se_{54}$	2.41	3.81	2.64
$Ge_{27}As_{37}Se_{36}$	2.45	3.87	2.91

However, the chemical local order around Ge and As was reported to be changed as the glasses changed from being Se-rich to Se-deficient. Ge atoms were found to be bonded only to Se atoms forming GeSe4 polyhedra in stoichiometric and Se-rich alloys, while they (Ge atoms) could be coordinated by both Se and X (X - Ge; As) atoms in Se-deficient glasses (Ge and As atoms were not distinguished) [31].

At low Ge concentration (and low MCN), there is minimal As−As homonuclear bonding. With increasing MCN, the Ge-As-Se glasses show an abrupt increase in As−As bonding after the Se-even stoichiometric transition at MCN = 2.60, mostly at the cost of As−Se bonds. This is supported by XRD measurements showing As−As homonuclear bonds dominating Ge−Ge bonds. Overall, the MCN roughly follows the trend expected by the 8 − N rule although the discrepancy tends to increase with increasing MCN.

Similar results were obtained in the research of structural order in $(As_2S_3)_x(GeS_2)_{1-x}$ and $(As_2S_3)_{100-}$

$_x(Sb_2S_3)_x$ glasses carried out in [36-38]. It is revealed [36-37] that the structural order of As-rich (x > 0.4) and Ge-rich (x < 0.4) glasses is organized by the main As-S and Ge-S structural motifs based on pyramidal AsS_3 and tetrahedral GeS_4 units linked by =As-S-As= and ≡Ge-S-Ge≡ structural configurations, respectively. While for the intermediate compound with x = 0.4 the structural network seems to be better homogeneous on the nanoscale due to appearance of ≡Ge-S-As= mixed structural configurations resulting in misbalance between corner-shared and edge-shared tetrahedral units in comparison with their predicted ratio for binary GeS_2 glass. The structure of this alloy is similar to the structure of the stoichiometric glass $Ge_{18.2}As_{18.2}S_{63.6}$ (i.e., x= 0.455) consisting of a coner-shared network of homogeneously mixed GeS4 tetrahedra and AsS_3 pyramids.

3.2. Raman spectra

The Raman spectra of Ge-As-Se samples presented in Fig. 3 exhibit main bands: 235-248 cm^{-1}, bands at 186-200 cm^{-1}, band at 258 cm^{-1} and a wide band structure around 107 cm^{-1}. Observed bands in the Raman spectra of Ge-As-Se samples can be explained in the terms of vibrational modes of As_2Se_3 and $GeSe_2$ glasses [12]. The band at 227 cm^{-1} in spectra, is ascribed to $AsSe_{3/2}$ pyramidal units [39]. The band at 237 cm^{-1} is attributed to the As_4Se_3 entities [39]. Additional band can be revealed at 258 cm^{-1}, it is assigned to the presence of Se-Se bonds [10, 40, 41].

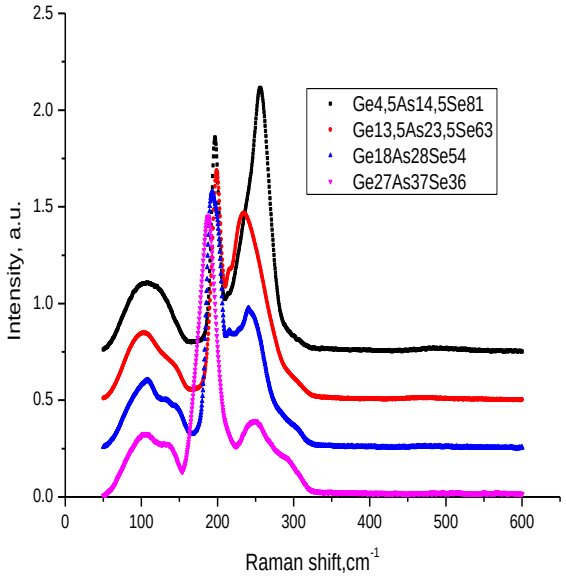

Fig. 3. Raman spectra of studied Ge-As-Se chalcogenide glasses (color online)

Gaussian decompositions of Raman spectra of $Ge_{13.5}As_{23.5}Se_{63}$ glass is shown in Fig. 4. This glass composition is close to the pseudo-binary cross-section $(GeSe_2)_x(As_2Se_3)_{1-x}$. Assignments of particular bands detected in Raman spectra of Ge-As-Se samples are summarized inTable 2.

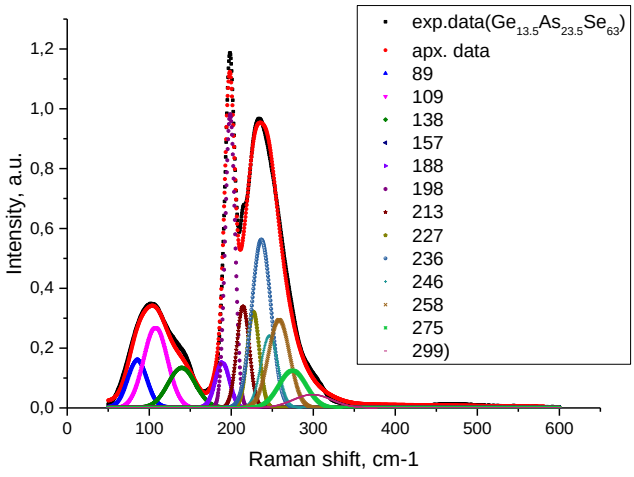

Fig. 4. Gaussian decompositions of Raman spectra of $Ge_{13.5}As_{23.5}Se_{63}$ glass (color online)

Table 2. Assignment of particular bands detected in Raman spectra of Ge-As-Se samples

Wavenumber, cm^{-1}	Assignment	References
100-200	Vibrations of structural units containing As-As and Ge-As bonds	[11, 42]
198	Vibrations of the corner-shared $Ge(Se_{1/2})_4$ tetrahedral units	[41,43, 44]
213	Vibrations of the edge-shared $Ge(Se_{1/2})_4$ tetrahedral units.	[43, 44]
227	Vibrations of the $AsSe_{3/2}$ pyramidal units	[12, 39]
237	Vibrations of the As_4Se_3units	[12, 39, 41]
245	Motion of As-Se bonds in As_4Se_4 structural units	[42]
258	Se-Se vibrations in the Se-chains	[10, 40, 41]
276	Vibrational mode of –Se-Se- bridges between $AsSe_3$ pyramidal units and As_4Se_4 or As_4Se_3 cages.	[39]
285 - 300	$GeSe_{4/2}$ tetrahedra asymmetric vibration	[45]

The broad band structure in the range of 60-180 cm^{-1} was described using the set of Gaussians at 89, 109, 138, 157 and 188 cm^{-1} (Fig. 4). The bands located in this region (Fig. 4) confirm the presence of structural units containing As-As bonds and Ge-As vibrations [11, 42]. One oscillator (Fig. 4) was used for modelling 198 cm^{-1} band. This band can be attributed to the formation of corner-shared $Ge(Se_{1/2})_4$ tetrahedral units [41, 43-44]. To describe the 200-300 cm_{-1} broad band we used six oscillators at 213, 227, 237, 245, 258, 276 cm^{-1} (Fig. 4) and 299 cm^{-1}. The band at 213 cm^{-1} is assigned to edge-shared $Ge(Se_{1/2})_4$ tetrahedral units. The Raman spectra of As_2Se_3glasses are characterized by a strong band at 227 cm^{-1} (Fig. 4), it is assigned to the vibrations of the $AsSe_{3/2}$ pyramidal units [39]. The band at 237 cm^{-1} (Fig. 4), may be attributed to As_4Se_3 structural unit containing As-As homopolar bonds, it is typical for Se-deficit alloys [39]. The band at 245 cm^{-1} can be assigned to the motion of As-Se bonds in As_4Se_4 structural units. The band at 258 cm^{-1} corresponds to the Se-Se vibrations in the Se-chains. The band at 276 cm^{-1} can be assigned to the vibrational mode of –Se-Se- bridges between $AsSe_3$ pyramidal units and As_4Se_4 or As_4Se_3 cages [39].

Tentative gaussian decompositions of Raman spectra of $Ge_{4.5}As_{14.5}Se_{81}$ glass is shown in Fig.5. As was expected for the Se-rich glasses we observe strong 258 cm^{-1} band characteristic for Se-Se vibrations in the Se-chains [10, 40, 41]. Here it is necessary to note, that bands characteristic for vibrations of the corner-shared and edge-shared $Ge(Se_{1/2})_4$ tetrahedral units [43, 44], vibrations of the $AsSe_{3/2}$ pyramidal units [12, 39] and structural units containing homopolar bonds [12, 39, 42].

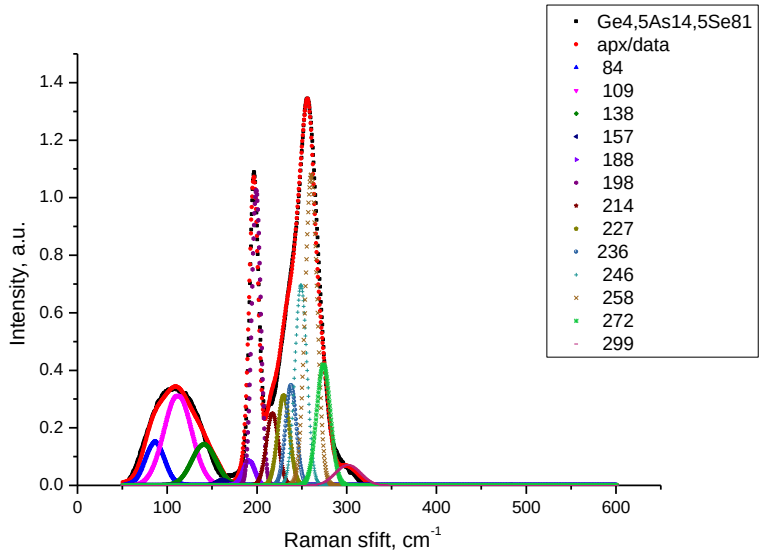

Fig. 5. Gaussian decompositions of Raman spectra of $Ge_{4.5}As_{14.5}Se_{81}$ glass (color online)

Tentative gaussian decompositions of Raman spectra of Se-deficient $Ge_{27}As_{37}Se_{36}$ glass is shown in Fig.6. Here 188 cm^{-1} band is the strongest. But also 258 cm^{-1} band corresponding to the Se-Se vibrations in the Se-chains [10, 40, 41] is present, as well as other bands corresponding to the structural units of As_2Se_3 and $GeSe_2$ glasses and structural units containing homopolar bonds (see Table 2).

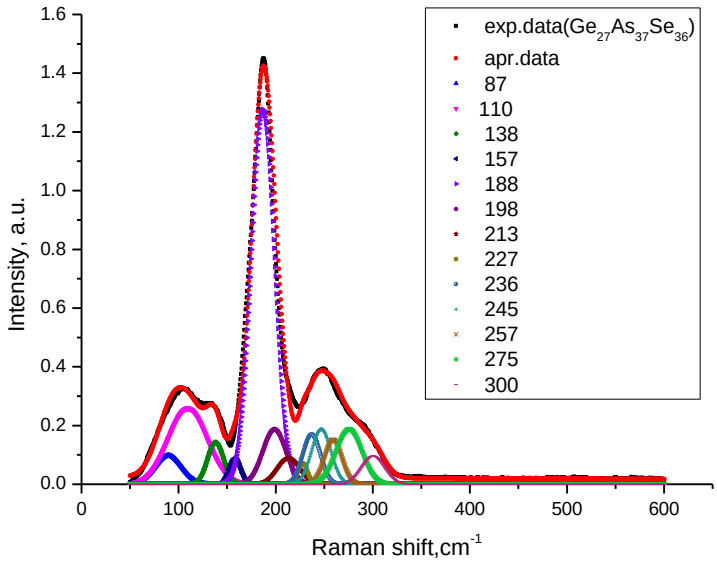

Fig. 6. Gaussian decompositions of Raman spectra of $Ge_{27}As_{37}Se_{36}$ glass (color online)

Compositional dependencies of the intensities of the characteristic Raman bands correlate with evolution of concentration of the different structural units in Ge-As-Se alloys along the studied compositions. Raman spectra of Ge-As-Se samples revealed that the backbones of the studied samples consist of $AsSe_{3/2}$ pyramidal units, edge- and corner-shared $GeSe_4$ tetrahedral units and structural units containing homopolar bonds. Compositional dependencies of characteristic constituent Raman bands intensities showed that Ge-As-Se samples contain different nanophases whose concentration is changing with composition. The shift of the bands in the Raman spectra of studied alloys can be interpreted in the term of the interplay of its component bands' intensities.

4. Conclusions

Radial distribution functions obtained for studied Ge-As-Se glasses ($Ge_{4.5}As_{14.5}Se_{81}$, $Ge_{13.5}As_{23.5}Se_{64}$, $Ge_{18}As_{28}Se_{54}$, and $Ge_{27}As_{37}Se_{36}$) have shown that positions of the nearest-neighbour bond length r1 changed from 2.32 to 2.45 Å with the increase of Ge content. Raman spectra of Ge-As-Se samples revealed that the backbones of the studied samples consist of $AsSe_{3/2}$ pyramidal units, edge- and corner-shared $GeSe_4$ tetrahedral units and structural units containing homopolar bonds. For Se-rich samples Se chains are present. Compositional dependencies of characteristic constituent Raman bands intensities showed that Ge-As-Se samples contain different nanophases whose concentration is changing with the composition.

References

[1] A. V Stronski, E. F. Venger, P. F. Oleksenko, O. V. Melnichuk, Chalcogenide vitreous semiconductors: properties and practical applications, NSU, Nizhyn, 236 (2016)
[2] R. P. Wang, Amorphous Chalcogenides, Jenny Stan, New York, 2013.
[3] H. H. M. Balyuzi, Acta Cryst. **A31**, 600 (1975).
[4] T. E. Faber, J. M. Ziman, Philosophical Magazine **11**(109), 153 (1965).
[5] O. Uemura, Y. Sagara, T. Satow, Physica Status Solidi A **26**(1), 99 (1974).
[6] N. Afify, A. Gaber, I. Abdalla, H. Talaat, Physica B: Condensed Matter **229**(2), 167 (1997).
[7] A. H. Moharram, A. M. Abdel-Basit, Physica B: Condensed Matter **358**(1-4), 279 (2005).
[8] T. Petkova, M. Mitkova, Mir.Vlček, S. Vassilev, J. Non-Cryst. Solids **326**(327), 125 (2003).
[9] A. Prasad, C. Zha, R. Wang, A. Smith, S. Madden, Opt. Express **16**, 2804 (2008).
[10] S. Xu, R. Wang, Z. Yang, L. Wang, B. Luther-Davies, Applied Physics Express **8**(1), 015504 (2015).
[11] C. Zha, R. Wang, A. Smith, A. Prasad, R. A. Jarvis, B. L. Davies, J. Mater. Sci. Mater. Electron. **18**, 389 (2007).
[12] K. Shportko, L. Revutska, O. Paiuk, J. Baran, A. Stronski, A. Gubanova, E. Venger, Optical Materials **73**, (2017) 489 (2017).
[13] A. Stronski, M. Vlček, Opto-electronics Review **8**(3) 263 (2000).

[14] G. Lucovsky, R. M. Martin, J. Non-Cryst. Solids **8e10**, 185 (1972).
[15] K. Tanaka, Phys. Rev. **39**, 1270 (1989).
[16] M. Thorpe, J. Non-Cryst. Solids **76**, 109 (1985).
[17] L.Cervinka, J. Non-Cryst. Solids **98**, 207 (1987).
[18] A.Stronski, L. Revutska, A. Meshalkin, O. Paiuk, E. Achimova, A. Korchovyi, K. Shportko, O. Gudymenko, A. Prisacar, A. Gubanova, G. Triduh, Optical Materials **V94**, 393 (2019).
[18] V. Bilanych, V. Komanicky, M. Kozejova, A. Feher, A. Kovalcikova, F. Lofaj, V. Kuzma, V. Rizak, Thin Solid Films **616**, 86 (2016).
[19] V. I. Minko, I. Z. Indutnyy, P. E. Shepeliavyi, P. M. Litvin, J. Optoelectron. Adv. M. **7**(3), 1429 (2005).
[20] A. Stronski, E. Achimova, O. Paiuk, A. Meshalkin, V. Abashkin, O. Lytvyn, S. Sergeev, A. Prisacar, P. Oleksenko, G. Triduh, J. Nano Res. **39**, 96 (2016).
[21] V. Kuzma, V. Bilanych, M. Kozejova, D. Hlozna, A. Feher, V. Rizak, V. Komanicky, J. Non. Cryst. Solids **456**, 7 (2017).
[22] A. Stronski, E. Achimova, O. Paiuk, A. Meshalkin A. Prisacar, G. Triduh, P. Oleksenko, P. Lytvyn, Nanoscale research letters **12**(1), 286 (2017).
[23] O. Shylenko, V. Bilanych, A. Feher, V. Rizak, V. Komanicky, J. Non. Cryst.Solids **505**, 37 (2019).
[24] L. Revutska, O. Shylenko, A. Stronski, V. Komanicky, V. Bilanych, Physics & Chemistry of Solid State **21**(1), 146 (2020).
[25] P. J. Webber, J. A. Savage, J. Non-Cryst. Solids **20**, 271 (1976).
[26] M. A. Popescu, Non-Crystalline chalcogenides (Kluwer Academic, Dordrecht, 2001).
[27] N. E. Cusack, D. L. Stein, The Physics of Structurally Disordered Matter: An Introduction. Physics, IOP Publishing Ltd., Bristol, England, 1987.
[28] A. Szczygielska, A. Burian, J. C. Dore, V. Honkimki, S. Duber, Journal of Alloys and Compounds **362**(1-2), 307 (2004).
[29] T. Proffen, S. J. L. Billinge, T. Egami, D. Louca, Z. Krist. **218**, 132 (2003).
[30] J. C. Phillips, J. Non-Cryst. Solids **34**, 153 (1979).
[31] I. Kaban, P. Jóvári, R. P. Wang, B. Luther-Davies, J. Phys.: Condensed Matter **24**(38), 385802 (2012).
[32] https://rad-gtk.software.informer.com/amp/
[33] I. Pethes, I. Kaban, R. P. Wang, B. Luther-Davies, P. Jóvári, Journal of Alloys and Compounds **623**, 454 (2015).
[34] I. Pethes, Journal of Alloys and Compounds **623**, 454 (2015).
[35] Ildikó Pethes, Radwan Chahal, Virginie Nazabal, Carmelo Prestipino, Angela Trapananti, Stefan Michalik, Pál Jóvári, J. Phys. Chem. B **120**, 9204 (2016).
[36] A. Stronski, T. Kavetskyy, L. Revutska, K. Shportko, M. Popovych, I. Kaban, P. Jóvári, Journal of Non-Crystalline Solids **572**, 121075 (2021).
[37] A. V. Stronski, T. S. Kavetskyy, L. O. Revutska, I. Kaban, P. Jóvári, K. V. Shportko, V. P. Sergienko, M. V. Popovych, Semiconductor Physics, Quantum Electronics & Optoelectronics **24**(3), 312 (2021).
[38] A. Stronski, L. Revutska, K. Shportko, O. Gudymenko, J. Baran, M. Trzebiatowska, P. Oleksenko, Functional Materials **27**(2), 315 (2020).
[39] M. S. Iovu, E. I. Kamitsos, C. P. E. Varsamis, P. Boolchand, M. Popescu, Chalcogenide Lett. **2**, 21 (2005).
[40] N. Mateleshko, V. Mitsa, M. Veres, M. Koos, J. Optoelectron. Adv. M. **7**, 139 (2005).
[41] O. V. Iaseniuc, M. S. Iovu, A.Pantazi, O. A. Lazar, C. C. Moise, M. Enachescu, Optoelectron. Adv. Mat. **15**(9-10), 498 (2021).
[42] M. K. N. Mateleshko, V. Mitsa, M. Veres, M. Koos, A. Stronski, Semicond. Phys. Quantum Electron. Optoelectron. **7**, 171 (2004).
[43] P. Nagels, R. Callaerts, R. Mertens, J. Phys. Iv **9**, 717 (1999).
[44] J. Orava, T. Kohoutek, T. Wagner, Z. Cerna, M. Vlcek, L. Benes, B. Frumarova, M. Frumar, J. Non. Cryst. Solids **355**, 1951 (2009).
[45] J. C. Olivier, P. Tchahame, P. Němec, M. Chauvet, V. Besse, C. Cassagne, G. Boudebs, G. Renversez, R. Boidin, E. Baudet, V. Nazabal, Opt. Mater. Express **4**, 525 (2014).

*Corresponding author: niva94@ukr.net